Computer Fraud and Security
ISSN (online): 1873-7056

A Precision Measuring Approach of Shaft Edge using Dual-stage Sub-pixel Detection with Lighting Compensation

Xiang Wu*, Junchao Wang, Zihan Zhang, Yuxin Zheng, Yaohuan Tan, Bingyang Guo
College of Electrical Engineering, Henan University of Technology, Zhengzhou, China
**Corresponding Author.*

Abstract:
This research introduces a method with a pragmatic approach for measuring the contour of shaft workpieces. The algorithm utilizes dual-stage Canny edge detection and sub-pixel localization techniques. This study focuses on the challenges associated with edge detection in the context of back-light lighting systems, with the aim of enhancing both accuracy and stability. The proposed technique integrates adaptive threshold-based Canny edge detection, weighted fusion, and morphological algorithms in order to improve the continuity of edges. The process of identifying the location of a coarse edge is accomplished through the utilization of cubic spline interpolation and curve fitting techniques to determine sub-pixel coordinates. The RANSAC fitting algorithm is employed to estimate lines that best match a set of edge points, hence enabling the computation of accurate values for axis-type components. The error analysis and compensation under various lighting conditions were completed through experimental analysis. The method described in this study demonstrates a notable level of accuracy and reliability in the recognition of cylindrical standard parts. It exhibits the capability of precisely identifying standard parts of varying sizes, with an absolute error margin of 8 micrometers. In addition, the algorithm has anti-interference capability, and we deployed the algorithm on Nvidia's Jetson orin nano, so that the entire system design can be more compact. In conclusion, this algorithm offers a viable solution for the efficient and accurate recognition of part contours in diverse settings.

Keywords: precision measurement, sub-pixel edge extraction, cubic spline interpolation, lighting compensation

INTRODUCTION

Machine vision is a highly promising technology in the field of precision inspection. It uses optical devices and non-contact sensors to capture characteristic images of the object being measured. The parallel computing capability of GPU platform can accelerate the execution of machine vision algorithms, thus improving the real-time and accuracy of the system [1]. Through computer simulations of human visual intelligence, it extracts and processes useful information from objective objects, ultimately applying it to practical detection and control processes. Due to its high precision in positioning, real-time capabilities, and high repeatability, machine vision systems were initially used primarily in industrial electronic defect detection and have gradually been applied to industries such as automotive, electronics, and electrical. The main applications of vision systems in industrial settings can be divided into three parts: automatic inspection, vision servo systems, and intelligent assembly. In automatic inspection, this includes automated visual recognition tests and geometric measurement tests, with geometric measurement technology being an indispensable part of part processing in the mechanical machining field.

In the field of mechanical machining, parts are crucial and common components. They play important roles in tasks such as motion transmission, fitting, and connection. The geometric dimensions and accuracy of parts directly affect the product's lifespan, performance, and condition. Therefore, optimizing the design and manufacturing processes of parts plays a vital role in reducing environmental pollution and energy consumption. Specifically, in mechanical machining, precise part dimensions ensure good fitting between parts, reducing friction and wear, thus extending the lifespan of parts and the entire system. For example, in bearings, insufficient part dimensional accuracy can lead to excessive clearance or overly tight fits, limiting the efficiency and lifespan of the bearing. However, currently, part dimension measurement in industrial settings mainly relies on traditional manual methods, such as vernier calipers and coordinate measuring machines. This detection method requires highly skilled operators, has high labor intensity, low inspection efficiency, and does not effectively ensure the quality of the products being inspected. Additionally, human errors exist, further reducing the reliability of inspections. Therefore, it is difficult to meet the requirements for high-precision, high-efficiency, and large-scale product inspections. Thus, researching high-precision and robust part inspection algorithms and building

corresponding inspection systems is of great significance to improve the technical level of the manufacturing industry. The automatic part inspection algorithm based on machine vision and image classification technology can effectively solve the shortcomings of traditional inspection methods [2,3]. By capturing part images and utilizing image processing and computer vision algorithms to extract feature information, rapid and highly accurate part inspection can be achieved. This algorithm is robust and reliable and is suitable for large-scale product inspection needs. Applying this algorithm can improve the accuracy and stability of part inspection, providing effective support for the development of the mechanical manufacturing industry and enhancing product quality and competitiveness. Currently, many researchers have used machine vision technology for industrial part dimension inspection.

For example,Bing [4] proposed a method for detecting the diameter of small glass beads based on digital image processing. This approach used the Sobel operator to calculate the gradient of the object to be measured, employed spatial moment sub-pixel localization algorithm for precise edge positioning, and experiments verified that the algorithm had low dependence on binarization threshold, high detection accuracy, and fast calculation speed. Yao [5] applied machine vision detection technology to develop a machine vision-based rolling bearing outer ring radius detection system. They used the Roberts operator to extract the edges of the bearing, followed by feature extraction of the workpiece, achieving stable and repeatable bearing inspection. Moru and Borro [6] and others addressed the expensive and time-consuming issues associated with traditional gear measurement methods by developing a machine vision-based gear parameter measurement system. The system segmented the gear's rough edges through pixel-based image segmentation and then obtained sub-pixel edges of the gear using interpolation, followed by detecting the inner and outer diameters and the number of teeth using different algorithms. Experimental results confirmed a minimum calibration error of 0.06 pixels, meeting the requirements for high-precision inspection.Chai [7] adopted a PIN detection method for ceramic antenna based on image processing. They use the improved Sobel operator and Gaussian peak position estimation subpixel edge detection algorithm, and use the least square method to simulate the edge points into a straight line to calculate the width. The experiment verifies that the algorithm has high accuracy and stability. Liu [8] et al. adopted the improved canny operator to realize the rough location of the pixel-level edge coordinates of the center of the circular hole for the circular hole type parts. Based on the Ghosal algorithm, they proposed a new edge judgment condition and calculated the optimal gray step threshold of Zernike moment by iterative method to judge and obtain the sub-pixel edge points. Finally, the center coordinates and radius of circular hole are detected and measured with high precision by the least square principle. The relative error of the improved algorithm is in the range of 0.02 pixels, and the relative error accuracy of the radius is in the range of 0.05 pixels.Numerous studies demonstrate that machine vision-based inspection technology offers fast inspection rates, high precision, and strong repeatability when inspecting parts.

The contribution of the paper is summarized below:

(1) Based on the edge equipment Jetson orin nano, a set of high-precision and stable shaft workpiece size detection instrument was designed.

(2) An adaptive Canny operator is proposed, and a comparison experiment with Sobel operator is done.

(3) A subpixel edge detection algorithm based on cubic spline difference is proposed.

(4) Evaluate the performance difference between this algorithm and Zernike algorithm and PAE before.

(5) Experiments have verified the performance of the proposed algorithm in detecting axisymmetric workpieces of different diameters and its good noise resistance.

OBJECTIVES

This paper introduces the development of a component measurement system based on edge device Jeston orin nano and backlight photography [9]. Its main function is image acquisition and result output. In terms of image capture, the system employs the Dahua A3B00MG000 industrial camera, which boasts a resolution of 5472×3648 pixels and pixel dimensions of $2.4\mu m \times 2.4\mu m$. The target surface size is 12.7mm ×9.6mm. This camera is capable of providing high-resolution images, meeting the requirements for capturing fine details of components. To mitigate the impact of depth of field on distortion, the Opto TC23048 double telecentric lens is used, offering a

magnification factor of 0.184 [10]. By calculating the field of view as the target surface size divided by the magnification factor, the system achieves a field of view measuring 69.217mm × 52.174mm. This field of view is sufficient for capturing local images of common components and their intricate details. Compared to diffused backlight illumination, telecentric illumination delivers higher edge contrast, thus enhancing measurement accuracy. To meet this requirement, the OPT-HZPXB parallel light source is employed as the backlight source. This light source provides high-quality parallel illumination, excelling in high-precision measurements of circular or cylindrical components [11]. The system is constructed as depicted in Figure 1. In the software component of the system, the authors utilize the C++ programming language in conjunction with two powerful libraries: OpenCV and Qt. OpenCV is a widely used computer vision library that offers a rich set of image and video processing capabilities [12]. Qt, on the other hand, is a cross-platform GUI development framework that enables the rapid construction of high-quality application interfaces. The integration of these two libraries allows for swift implementation of detection and measurement for various parts of the components under inspection. Through the combination of the aforementioned hardware and software components, the component measurement system described in this article is capable of high-resolution image capture. It further achieves precise component measurement and inspection through image processing and computer vision algorithms.

The algorithm in this article is mainly divided into two steps for measuring parts. The first step is the edge coarse positioning phase, whose primary purpose is to apply an improved Canny algorithm to the ROI (Region of Interest) of the part to obtain preliminary contour information. The next step is the image fusion phase, which uses pixel-weighted averaging to fuse the edge-extracted image obtained from coarse positioning with the binary image of the original image. Finally, sub-pixel edge coordinates of the part are obtained using a cubic spline interpolation algorithm, and the RANSAC fitting algorithm [13,14] is used to fit these coordinates into straight lines, thus achieving the measurement of the part's dimensions.

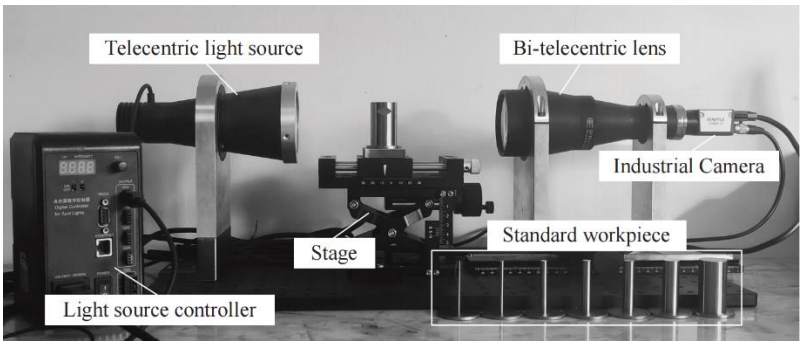

Figure 1. Detection system

ADAPTIVE CANNY EDGE DETECTION ALGORITHM

The Canny operator is a widely used edge detection algorithm in the field of image processing and computer vision, known for its noise resistance and ability to preserve fine details. Compared to the Sobel [15] and Laplacian operators [16], the Canny operator effectively reduces the influence of noise on edge detection and extracts clearer and finer edge lines by sacrificing computation time. Traditional Canny operators use Gaussian filtering for noise reduction, but this can result in edge blurring and the loss of a significant amount of edge information [17]. This algorithm replaces the Gaussian filtering in the traditional Canny operator with bilateral filtering to achieve better filtering results and preserve edge information to the maximum extent.

Additionally, in the double threshold detection step, traditional methods often use manually selected thresholds, which are empirical choices for the best values. However, in industrial inspections, complex real-time environmental conditions make it difficult to quickly find suitable thresholds. Therefore, an adaptive threshold algorithm is needed to select appropriate edge points.

The algorithm flow for edge detection using the adaptive Canny operator can be briefly divided into four steps: bilateral filtering, gradient calculation, non-maximum suppression, and double threshold detection. The specific steps are as follows:

(1) In a color image, each color channel may contain a different noise pattern.When the image is converted to grayscale, the differences between these channels can be eliminated, making the noise more consistent and easier to handle in a single channel.To reduce the impact of noise on the edge detection results, first select the ROI region and convert the image to grayscale, and then smooth the image using bilateral filtering.

(2) Calculate the horizontal gradient value G_x and vertical gradient value G_y at each point in the image using edge gradient operators, resulting in the gradient magnitude G and gradient direction θ at each point.

$$\begin{aligned} Gradient &= \sqrt{G_x^2 + G_y^2} \\ Angle(\theta) &= \arctan\left(G_y/G_x\right) \end{aligned} \tag{1}$$

(3) Find local gradient maxima along the gradient direction at each point and suppress non-maximum elements to preserve the fine details of the edges.

(4) After non-maximum suppression in step (3), some noise may still exist. To further extract edges, the OTSU [18] algorithm is used to determine the high threshold for double threshold detection. To supplement weak edges that may be missed by high thresholds and reduce the impact of noise, we employ a balancing strategy where the low threshold is set to half the high threshold.It can reduce the possibility of noise being mistakenly detected as edge to some extent,resulting in clear image edges.

The original image of the ROI region of the test object, the Sobel operator edge detection image, and the edge image extracted using the adaptive threshold Canny operator are shown in Figure 2. Compared to the Sobel operator's detection, the adaptive threshold Canny operator provides more complete edge information with fewer false edges.

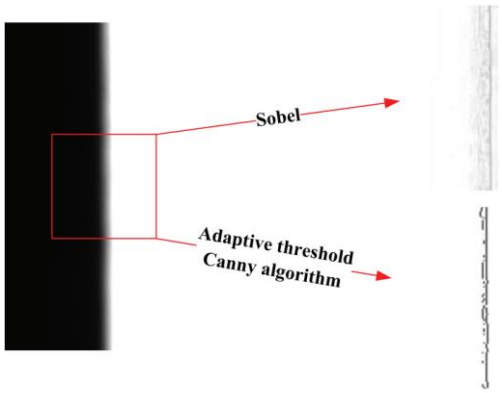

Figure 2. Original image and edge detection results

Sub-pixel Edge Detection Using Cubic Spline Interpolation Fitting Algorithm

In adaptive Canny edge detection, phenomena such as edge blurring caused by diffuse lighting, as shown in Figure 3, can still lead to the presence of false edges, affecting the accuracy of the edge localization algorithm. Directly calculating the part's dimensions by fitting lines to this image results in relatively large absolute accuracy errors and lower repeatability accuracy.

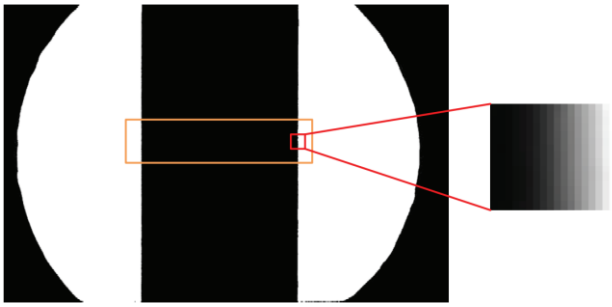

Figure 3. Image region of interest and localized zoom-in image

To achieve more accurate part edge extraction, this paper proposes a sub-pixel edge detection algorithm based on cubic spline interpolation. First, the extracted edge information is weighted and fused with morphological operation results of the original image using an image fusion approach, and the image is filled. Next, the adaptive Canny algorithm is used for coarse edge localization, followed by the use of the cubic spline interpolation algorithm to obtain sub-pixel coordinates of the image edges. Finally, edge points are fitted with a straight line using the RANSAC fitting algorithm, and, considering the relationship between pixel coordinates and world coordinates, the actual dimensions of the part are determined. The algorithm flowchart is shown in Figure 4.

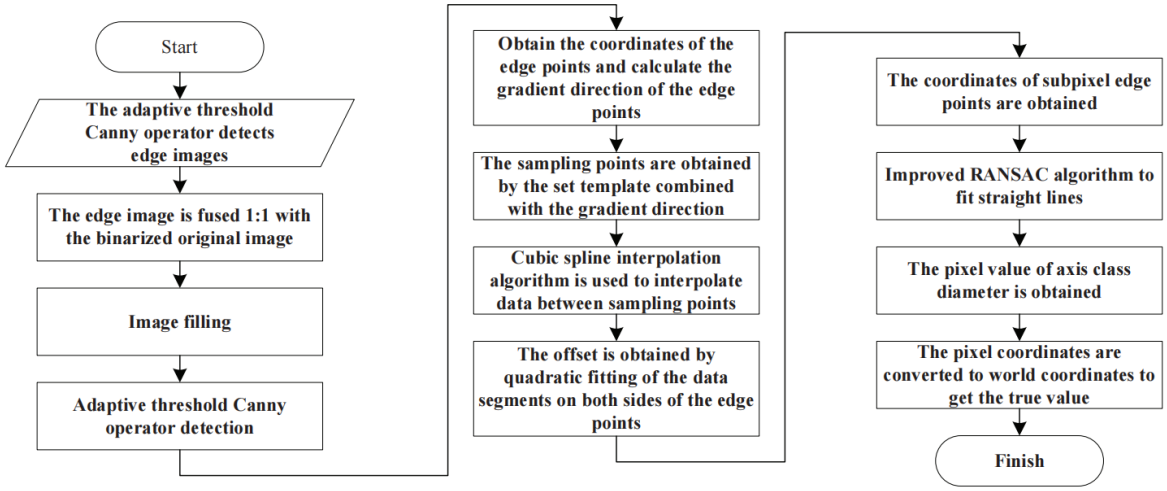

Figure 4. Part dimension inspection process based on image fusion and cubic spline interpolation algorithm

(1) Image fusion is performed using α * Edge detection image by the adaptive Canny algorithm + (1-α) * the original image, considering that both the original image and the edge image contain important feature information, they are of equal importance,so α = 0.5. Subsequently,in order to smooth the image and remove possible noise, the fused image is opened.

(2) The adaptive threshold Canny operator is applied to the fused image for edge detection, and the detection results are shown in Figure 5. The quality of edge detection significantly improves after the secondary detection, eliminating false edges and noise.

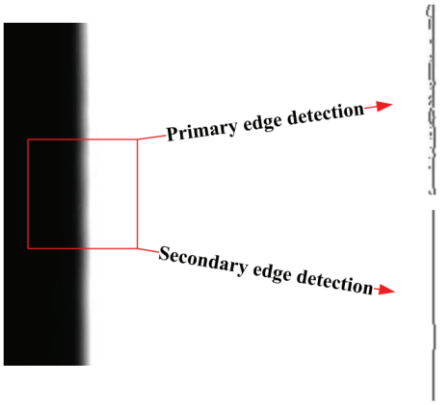

Figure 5. Comparison of edge detection results using adaptive Canny algorithm

(3) After obtaining accurate edges, pixel-level contour distance detection for the part can be performed. However, in engineering applications, pixel-level edge detection cannot meet the requirements of measurement accuracy, necessitating sub-pixel edge point localization [19]. Common sub-pixel edge detection algorithms include Zernike moments [20] and polynomial fitting [21]. After a comparative analysis, this paper ultimately selects the cubic spline interpolation algorithm for calculating sub-pixel edge point offsets. The specific process is as follows: first, extract the image's gradient magnitude and direction, with the gradient magnitude serving as the input to the fitting function. Using the fitting function, the edge point offset along the gradient direction, denoted as $offset$ can be

obtained. Then, by multiplying the offset with the gradient direction, the offsets in the x and y directions for the edge points are calculated. Adding these offsets to the pixel coordinates of the edge points yields the coordinates of the sub-pixel edge points. Figure 6 illustrates this process, where the the enlarged area on the right shows a specific edge pixel. By obtaining the edge point's $offset$, the sub-pixel edge point in the image can be calculated.

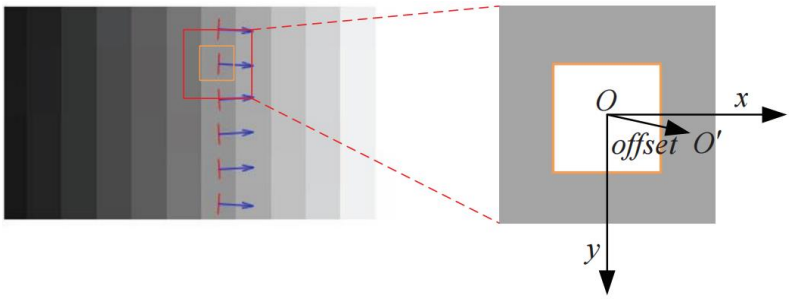

Figure 6. Sub-pixel edge point coordinate offset

(4) Increasing the number of selected neighboring pixel points during the cubic spline interpolation process helps provide more comprehensive information, further enhancing the accuracy and smoothness of the interpolation results. However, an excessive number of data points can lead to increased algorithm complexity and the potential introduction of unnecessary noise or overfitting issues. Additionally, the fitting error of cubic spline functions is closely related to the shape of the curve being fitted, making them suitable for smoothly varying curves but often resulting in larger fitting errors at positions where the curve shape changes significantly [22]. Therefore, the number of surrounding pixel points can be determined based on the steepness of the image gradient values. If the gradient changes are very steep, more pixel points are selected for interpolation calculations.The initial sampling template M of the algorithm is set to [-2 -1 0 1 2].When the gradient values of the edge point differ significantly from the gradient values of its surrounding sampling points, the sampling template range is expanded to ensure the reliability of the interpolation result.Let the pixel coordinates of the image's edge points be(x_i, y_i), the gradients be (Gx_i, Gy_i), and the gradient direction be θ_i, where$i = 1,2, \dots, n$, and n is the number of edge points in the image. Once the edge point positions are determined, the confirmation of sampling points $(X_{(i,j)}, Y_{(i,j)})$ is done based on the sampling template and gradient direction, computed as follows:

$$X_{(ij)} = M * sin(\theta_i) + x_i, Y_{(ij)} = M * cos(\theta_i) + y_i \tag{2}$$

where, j = 1, 2, 3, 4, 5.

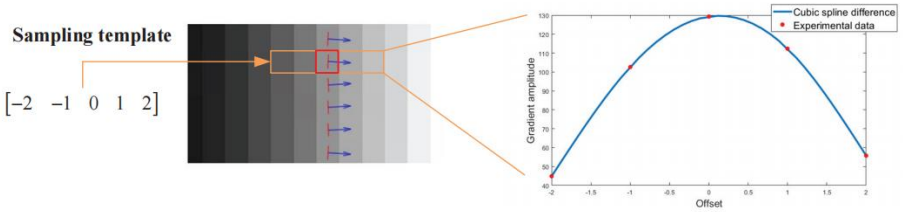

Figure 7. Edge point sampling and interpolation results

(5) After selecting the sampling points, the cubic spline interpolation method is employed for interpolating gradient values to obtain a smooth curve and reconstruct image data. The default sampling template M used in this paper contains a total of five sampling points, dividing the sampling space into four intervals. A cubic function is constructed for each interval, resulting in a total of i functions. The cubic function expression $f_{(i,j)}(k)$ for each interval is:

$$\begin{aligned} f_{(i,j)}(k) &= a_{(i,j)} + b_{(i,j)} * (k - X_{(i,j)}) + \\ & c_{(i,j)} * (k - X_{(i,j)})^2 + d_{(i,j)} * (k - X_{(i,j)})^3 \end{aligned} \tag{3}$$

Where k represents the point that needs interpolation, with $X_{(i,j)} \le k \le X_{(i,j+1)}$,and $j = 1,2,3,4,5$ .The coefficients $a_{(i,j)} b_{(i,j)} c_{(i,j)} d_{(i,j)}$ need to be determined.

In accordance with the following requirements, data interpolation is completed, and the interpolation results are shown in Figure 7:

I. At the sampling points, the function values are equal to the given data point values.

II. Function value continuity: Except for the first and last two sampling points, the spline function should exhibit zero-order continuity at the sampling points, meaning that the function value at that point is equal to the function value of the next data point at that point.

III. First derivative continuity: Except for the first and last two sampling points, the spline function is first-order continuous at all sampling points.

IV. Second derivative continuity: Within two sampling point intervals, the spline function ensures second-order continuity.

(6) After performing interpolation using the cubic spline interpolation algorithm, a quadratic function is used to fit the gradient value changes in the image's edge transition region. The expression of the fitted quadratic function is denoted as $H(t) = at^2 + bt + c$, where t represents the coordinate value along the gradient direction of the edge point, and a, b, and c are the parameters to be computed. $H(t)$ represents the gradient value of the edge, and when it reaches its maximum, the corresponding t is the optimal position of the edge in relation to the offset from the existing edge point. Therefore, it is necessary to calculate the equation coefficients to obtain the offset corresponding to the maximum value of the equation, which is calculated as $offset = -\frac{b}{2a}$.

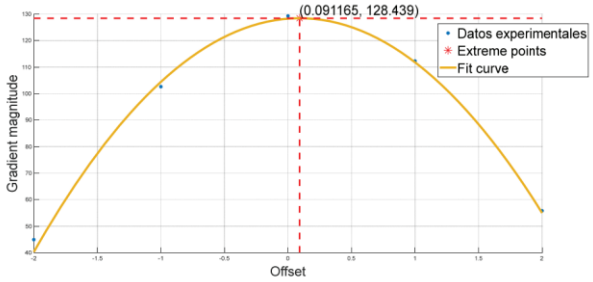

Figure 8. Gradient curve fitting and offset calculation

Figure 8 shows the results of fitting the curve of coordinate values and gradient magnitude for a specific point. The magnitude of the curve's maximum point relative to the original edge point is $offset = 0.091165$. From this, the sub-pixel edge coordinates in the gradient direction coordinate system are obtained. At this point, it is necessary to further transform them into the image coordinate system. Assuming that the integer part of the $offset$ is $offset_{int}$ and the decimal part is $offset_{dec}$, the expression for $offset$ is as follows:

$$offset = offset_{int} + offset_{dec} \tag{4}$$

Let the sub-pixel coordinates in the image edge be (x_{sub}, y_{sub}). The calculation formula is as follows:

$$x_{sub} = x_i + offset_{dec} * \cos(\theta_i), y_{sub} = y_i + offset_{dec} * \sin(\theta_i) \tag{5}$$

Thus, the sub-pixel edge coordinates of the tested component have been obtained, as shown in the following Table 1:

Table 1. A comparative analysis of subpixel and pixel coordinates

Pixel Coordinate	Subpixel Coordinates
(933,57)	(933.310,57.057)
(933,58)	(932.671,57.918)
(933,59)	(932.767,58.957)
(933,60)	(932.596,59.964)
(933,61)	(932.525,60.989)

(7) After obtaining sub-pixel edge coordinates, a straight-line fitting method can be used to fit the contour of the tested component and calculate the contour distance. The least squares method is an approach for determining a function model of a line based on minimizing the sum of squared residuals, but it is susceptible to the influence of discrete noise points. Therefore, the RANSAC fitting algorithm is chosen for line fitting. The main steps of this algorithm are as follows:

I. Set the number of iterations and a threshold.

II. Repeat the following steps until the specified number of iterations is reached:

a. Randomly select a sufficient number of samples from the original data for model fitting.b. Fit a model using the selected samples.c. Calculate the fitting error of all other data points to this model.d. Based on the threshold, mark data points with fitting errors less than the threshold as inliers and others as outliers.e. If the number of inliers exceeds the predefined threshold, consider the model as valid and terminate the iteration.

III. After reaching the specified number of iterations, re-fit a final model based on the model with the most inliers among all valid models.

IV. Return the final fitting model.

By completing these steps, the straight-line fitting of the tested component's contour is accomplished, and combined with calibration parameters, the actual diameter size of the tested workpiece is obtained.

The Algorithm Validation in This Article

To validate the performance of the algorithm presented in this article, a series of experiments will be conducted to assess the effectiveness of the proposed algorithm. These experiments are divided into three aspects. First, a comparative experiment will be performed to evaluate the performance differences between the algorithm presented in this article and the Zernike algorithm and the Local Gray Moment algorithm (PAE).Secondly, the article will demonstrate the performance of the proposed algorithm in the detection of axially symmetric test objects of different diameters (10mm, 25mm, and 40mm), verifying its applicability and evaluating its performance when dealing with objects of different sizes.Finally, experiments will be conducted to test the algorithm's noise resistance. The article will use the proposed algorithm to perform edge detection and contour distance measurement on original images of test regions with added Gaussian noise and salt-and-pepper noise of varying intensities. This experiment will assess the algorithm's robustness in the presence of noise and evaluate its reliability in practical applications. The article used the algorithm proposed in this article, as well as the Zernike algorithm and the Local Gray Moment algorithm (PAE) [23], to perform edge detection on 100 images of the same test objects, and the results were compared.

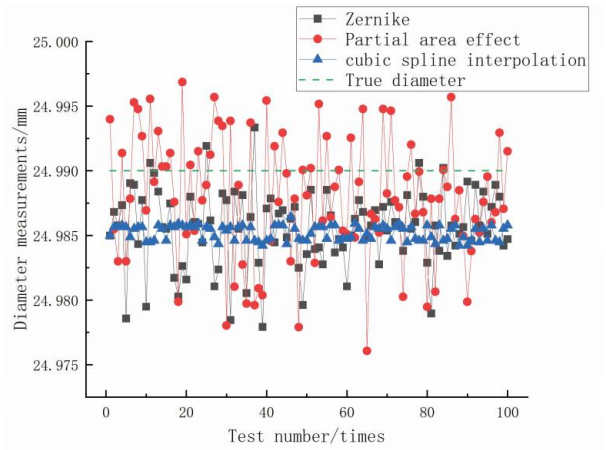

Figure 9. Comparison of different algorithm detection results

Figure 9 displays the detection results of three different algorithms. The Zernike algorithm's detection results, on the whole, are closer to the actual values of the cylinder. However, the sub-pixel edge detection algorithm based on second-order edge detection and third-order spline interpolation demonstrates the best stability. The

repeatability error after 100 detections is only 0.000056, whereas the corresponding values for the Zernike algorithm and the PAE algorithm are 0.000298 and 0.000478, respectively. Consequently, the algorithm presented in this article can achieve higher accuracy and stability through error compensation. Additionally, Table 2 shows that the algorithm in this article has superior computational efficiency when compared to the other two algorithms. It can provide rapid and accurate detection, making it more suitable for industrial applications.

Table 2. Comparison table of the time consumed by edge detection algorithms (s)

Zernike	Partial area effect	The algorithm
102.17	73.71	48.57

Another experiment aims to evaluate the performance of the algorithm proposed in this paper for the detection of cylindrical standard specimens with varying diameters. The experimental results are illustrated in Figure 10. Cylindrical standard components with nominal diameters of 10mm, 25mm, and 40mm (actual diameters of 9.99mm, 24.99mm, and 39.98mm, respectively) were selected as test objects, and 100 detections were performed. The differences between each detection result and the actual diameter were recorded and analyzed. The results indicate that the algorithm presented in this article achieved the best performance in the detection of the 25mm diameter cylinder. The average difference remained stable between 4-6 micrometers, demonstrating high accuracy. For the detection of a cylindrical object with a diameter of 40mm, the system stabilizes at approximately 6 micrometers, indicating excellent algorithmic stability. The algorithm presented in this article exhibited excellent performance for cylindrical standard components of different diameters, with detection errors within 8 micrometers, meeting the requirements for industrial use.

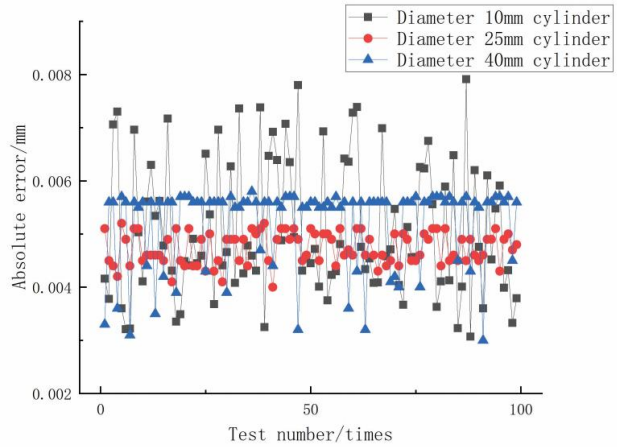

Figure 10. Test results of different standard parts

In order to assess the robustness of the algorithm in the presence of noise interference, various intensities of Gaussian and salt-and-pepper noise were introduced into the original images of the test area. Subsequently, edge detection and contour distance measurements were performed using the algorithm proposed in this paper, and the results are depicted in Figure 11. Observing and analyzing the experimental results, the following conclusions can be drawn.From the figures, it can be observed that even when adding Gaussian noise with intensities of 0.002 and 0.004, the algorithm presented in this article still demonstrates good noise resistance and exhibits minimal error in contour distance measurement. Furthermore, for salt-and-pepper noise, the algorithm also shows good stability. Despite the presence of a small amount of salt-and-pepper noise in the images, it is still able to accurately detect edges and perform contour distance measurements. This indicates that the algorithm presented in this article can, to a certain extent, overcome the impact of salt-and-pepper noise, maintaining a high level of robustness.For high-intensity noise situations, while the algorithm can provide some level of suppression, there are still some errors. High-intensity noise can have a significant impact on measurements, leading to increased uncertainty in the results.

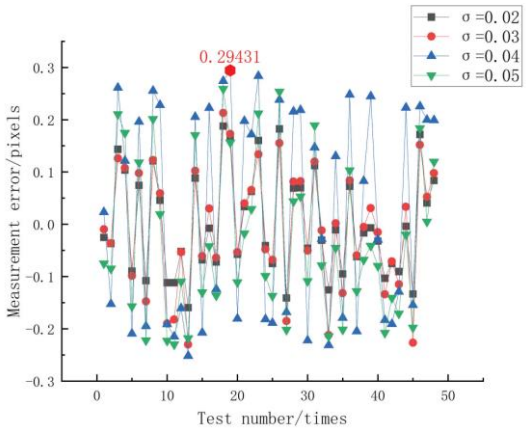

(a) Gaussian noise

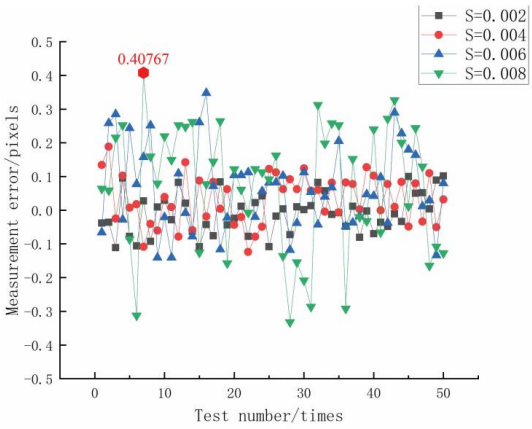

(b) Salt-and-pepper noise

Figure 11. Different intensity Gaussian noise and salt-and-pepper noise detection results of the algorithm in this paper

In summary, the algorithm presented in this article demonstrates outstanding accuracy and stability in detecting standard components of various sizes. It exhibits robustness in the face of certain levels of Gaussian noise and salt-and-pepper noise, maintaining a high level of resistance to disturbances.

Impact and Compensation of Lighting Conditions

Due to environmental factors and limitations of sensors or devices themselves, the lighting conditions of the detection system may vary, affecting the accuracy of sub-pixel edge positioning and ultimately influencing the results of size measurements. Figure 12 shows the absolute errors in the detection results of different diameter standard components at levels 15-20 after system calibration with the light intensity controller set at 18. Absolute error is the absolute value of the difference between the measured value and the true value. It reflects the magnitude of the deviation of the measured value from the true value.The figure clearly demonstrates significant differences in the detection results of the system under different lighting conditions.As the light intensity increases, the contrast between the edge of the workpiece and the background will gradually increase.However, it is important to note that this increase is usually limited and is affected by factors such as camera resolution, image processing algorithms, and so on. While the increase in light intensity helps to improve the contrast and sharpness of the edges, too much light can also cause more noise in the image. This is because the bright light may overheat or saturate the camera sensor, creating additional noise.

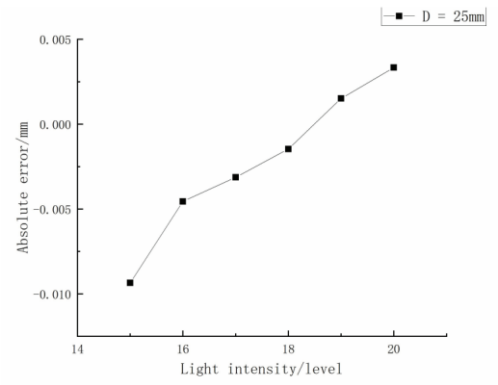

Figure 12. Detection results of the 25mm workpiece at different levels of the light source controller

Assuming the standard value of the workpiece is V, the light intensity is I_i, and the corresponding measurement result is V_i, the initial pixel equivalent value is K. The pixel equivalent value corresponding to the light intensity I_i is given by:

$$K_i = K \times \frac{V}{V_i} \tag{6}$$

To obtain pixel equivalent values under different light intensities, a mathematical model $M(I)$ needs to be constructed. Considering that establishing an accurate model between light intensity and pixel equivalent is complex, according to the Weierstrass First Approximation Theorem, it is possible to approximate using a polynomial sequence $K(I)$, i.e.:

$$M(I) \approx K(I) = a_0 + a_1 I + \ldots\ldots + a_n I^n = \sum_{k=0}^{n} a_i I^k \tag{7}$$

Since higher-order polynomials may cause oscillations, a lower-degree polynomial is generally chosen for approximation. In this paper, a quadratic function equation is used to fit the detection error caused by changes in light intensity, namely:

$$\begin{bmatrix} \sum_{i=1}^{n} 1 & \sum_{i=1}^{n} I_i & \sum_{i=1}^{n} I_i^2 \\ \sum_{i=1}^{n} I_i & \sum_{i=1}^{n} I_i^2 & \sum_{i=1}^{n} I_i^3 \\ \sum_{i=1}^{n} I_i^2 & \sum_{i=1}^{n} I_i^3 & \sum_{i=1}^{n} I_i^4 \end{bmatrix} \begin{bmatrix} a_0 \\ a_1 \\ a_2 \end{bmatrix} = \begin{bmatrix} \sum_{i=1}^{n} K_i \\ \sum_{i=1}^{n} K_i I_i \\ \sum_{i=1}^{n} K_i I_i^2 \end{bmatrix} \tag{8}$$

Substituting the values of Ii and Kiinto the above system of equations, the coefficients a2, a1, a0 can be solved. Based on actual measurement data, the calculated values are $a_2 = 0.001397, a_1 = 0.024483, a_0 = 12.9917$. Therefore:

$$M(I) \approx K(I) = 0.001397I^2 + 0.024483I + 12.991707 \tag{9}$$

The polynomial approximation curve is shown in Figure 13 demonstrating a good approximation effect that effectively reflects the relationship between light source intensity changes and pixel equivalent values.

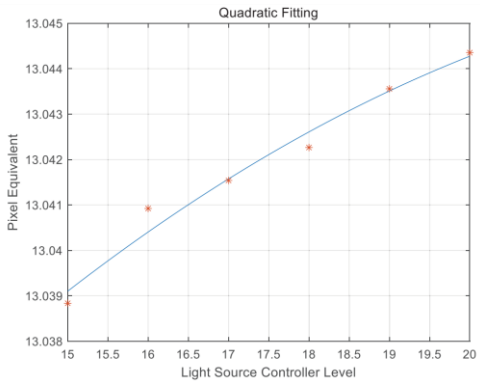

Figure 13. Relationship between pixel equivalent and light intensity

By fitting the relationship between light intensity and pixel equivalent, the compensation for workpiece detection results under different lighting conditions is ultimately achieved. Figure 14 displays the comparison of results before and after compensation. It can be observed that the change in lighting conditions after compensation does not significantly affect the detection results, leading to an improvement in system stability.

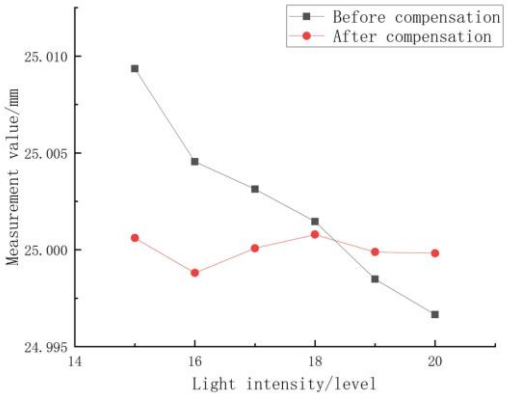

Figure 14. Comparison of results before and after lighting compensation

RESULTS

The primary objective of this paper is to address the demand for non-contact, high-precision detection in industrial applications, and a detection system based on dual telecentric lenses has been successfully developed. In the complex industrial inspection environment, where noise and illumination interference exist, an industrial parts detection algorithm based on second-order Canny edge detection and sub-pixel positioning is proposed. The algorithm initially employs the Canny edge detection algorithm with adaptive thresholds for the initial edge detection of the target image. Subsequently, the extracted edge information is fused with the original image using a weighted fusion method, followed by rough edge localization processing. Next, a third-order spline interpolation algorithm is utilized to obtain edge gradient interpolation information, and sub-pixel level coordinate information is obtained through curve fitting. This process yields the actual measurement values of the test piece, successfully compensating for errors under different lighting conditions.

Research results demonstrate that the proposed algorithm exhibits significant effectiveness in achieving measurement accuracy up to 8 micrometers for various sizes of standard specimens. Extensive repeated experiments show that the algorithm possesses high repeatability and a certain degree of interference resistance, meeting the requirements of industrial inspection scenarios. However, the system in this study responds to changes in ambient light passively. Future research could consider introducing methods that actively respond to changes in ambient light intensity, thereby optimizing the system's applicability.

REFRENCES

[1] Gajger, T. NVIDIA GPU Performance Monitoring using an Extension for Dynatrace OneAgent.Scalable Comput. Pmct. Erp.. 21 pp.689-699 (2020).
[2] Hemalatha, P., Shankar, G.& D.M, D.A New Improved Binary Convolutional Model for Classification of lmages. Scalable Computing: Practice And Erperience. (2022).
[3] Karthikeyan, A., Pavithra, S.& Anu, P. Detection and Classification of 2D and 3D HyperSpectral Image using Enhanced Harris Corner Detector. Scalable Computing: Practice AnaErperience.21 pp.93-100(2020).
[4] Bing-zhen, W. Image measurement for the diameters of micro glass spheres. Opto-electronic Engineering. (2005).
[5] Yao-nan, W. Rolling Bearing Outside Diameter Inspection System Based on Machine Vision.Computer Simulation. (2007).
[6] Moru, D. & Borro, D. A machine vision algorithm for quality control inspection of gears. International. Journal of Advanced Manufacturing Technology.106 (2020).
[7] Chai. PIN on-line precision detection of ceramic antenna based on improved subpixel algorithm Journal of Electronic Measurement and Instrumentation. 37, 170 (2023).

[8] Liu Liping, Sun Jian & Sun Wenyue Improved sub-pixel round hole part measurement methodof Zernike moment Improved sub-pixel round hole part measurement method of Zernikemoment.electron measure technology.46, 69-77 (2024).
[9] Indragandhi, K.& Jawahar, P. An Application based Efcient Thread Level Parallelism Schemeon Heterogeneous Multicore Embedded System for Real Time Image Processing. Scalable Computing: Pmctice and Erperience.
[10] Schuster, N. & Schoenheit, T. Infuence of the machine vision lens to the accuracy in contactless2D-metrology. Optomechatrnic Systems II. (2002).
[11] Pan, B., Yu, L. & Wu, D. High-accuracy 2D digital image correlation measurements using low cost imaging lenses: implementation of a generalized compensation method. MeasurementScience And Technology. 25, (2014).
[12] Zelinsky, A. Learning OpenOV-Computer Vision with the OpenOV Library (Bradski, G.R. etal.; 2008) [On the Shelf,. IEEE Robotics 8 Automation Magazine. 16 pp.100-100 (2009).
[13] Deng, J.& Han, Y. A real-time system of lane detection and tracking based on optimizedRANSAC B-spline fitting. Research In Adaptive And Convergent Systems. (2013).
[14] Zhou, K, Ye, G., Gao, X., Zhong, K., Guo, J.& Zhang, B. Weld Bead Width and HeightMeasurement Using RANSAC. 2019 4th International Conference On Control And RoboticsEngineering (ICCRE). pp. 35-39 (2019).
[15] Kanopoulos, N., Vasanthavada, N. & Baker, R. Design of an image edge detection filter usingthe Sobel operator. IEEE, Journal of Sold-State Circuits. 23, 358-367 (1988).
[16] Torre, V.& Poggio, T. On Edge Detection. IEEE Trnsactions On Pattern Analysis AnaMachine Intelligence.PAML-8, 147-163 (1986).
[17] Duan H, Shao H, Zhang S, et al. An Improved Algorithm for Image Edge Detection Based on Canny Operator. (2016).
[18] Yousef. J. lmage binarization using Otsu thresholding algorithm. Ontario, Canada: Universit! of Guelph.10 (2011).
[19] Jing, J., Liu, S., Wang, G., Zhang, W.& Sun, 0. Recent advances on image edge detection: A comprehensive review. Neurocomputing. 503 pp. 259-271 (2022).
[20] Ying-Dong, Q, Cheng-Song, C., San-Ben,0. & Jin-Quan, L. A fast subpixel edge detectionmethod using SobelZernike moments operator. Image And Vision Oomputing. 23, 11-17(2005).
[21] Xu, G. Sub-pixel Edge Detection Based on Curve Fitting. 2009 Second International ConferenceOn Information and Computing Science. 2 pp. 373-375 (2009).
[22] Zhi-xi, L. Analysis of the distribution effects of fitting nodes based on the cubic spline function. lournal Of Fujian College of Architecture 8 C.e. (2005).
[23] Trujillo-Pino, A., Krissian, K., Alemán-Flores, M.& Santana-Cedrés, D. Accurate subpixel edgelocation based on partial area effect. Image And Vision Computing. 31, 72-90 (2013).